Perturbation Analysis and Modeling of Curved Microstrip Bends

ANDREAS WEISSHAAR AND VIJAI K. TRIPATHI, SENIOR MEMBER, IEEE

Abstract —**The frequency-dependent transmission properties of the curved microstrip bend are derived by utilizing a second-order perturbation analysis of the equivalent modified curved waveguide model and a mode-matching method which includes the higher order modes. The scattering parameters of typical curved microstrip bends in (M)MIC's are computed and compared with those of the right-angle and chamfered right-angle microstrip bends. The calculations for the scattering parameters of the curved microstrip bends exhibit good convergence behavior with increasing number of higher order modes considered. The results are consistent for large curvatures and bends with small angle.**

I. Introduction

THE MAGNETIC wall waveguide model for a microstrip line [1] together with the mode-matching method proposed by Kühn [2], [3] has been successfully used in the past to analyze microstrip discontinuities such as impedance steps, bends, and T junctions [3].

In this paper the curved microstrip bend consisting of a microstrip ring segment between two microstrip lines is analyzed for its transmission properties. The microstrip lines are modeled by equivalent ideal magnetic wall waveguides [1] for which the electromagnetic field solutions are known [3]. The field solutions in the microstrip ring segment are derived by utilizing a perturbation analysis [4] of a modified (magnetic wall) curved waveguide model. Other techniques have been formulated to evaluate the fields inside curved metallic waveguides. These include the use of an equivalent nonuniformly loaded straight waveguide [5] and the rectangular and annular modal analysis [6]. The perturbation solution for the fields in the equivalent curved waveguide model developed here is readily adaptable to the mode-matching procedure and is used to calculate the properties of the curved microstrip bend discontinuities. The frequency-dependent reflection and transmission coefficients of curved microstrip bends are determined and compared with those of the right-angle and chamfered right-angle microstrip bends [7]–[9].

II. Theory

The curved microstrip bend is shown in Fig. 1. It consists of a microstrip ring segment (region III) with angle α and radius R which connects two microstrip lines

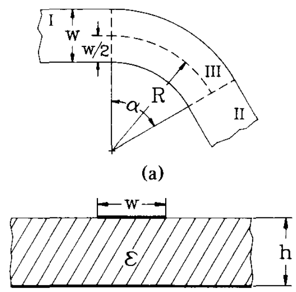

Fig. 1. The curved microstrip bend: (a) top view; (b) cross-sectional view.

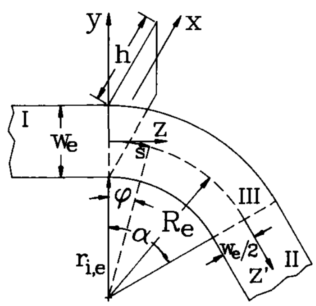

Fig. 2. The curved equivalent waveguide model for the microstrip bend.

(regions I and II) with width w on a substrate of height h and permittivity ϵ. The corresponding magnetic wall waveguide model for the microstrip lines, shown in Fig. 2, is characterized by its frequency-dependent effective width w_e and effective permittivity ϵ_e (e.g., [10]). Since the curved microstrip bend contains no discontinuities in width and permittivity (i.e., has constant width w and permittivity ϵ), a modified (magnetic wall) curved waveguide model is used here for the microstrip ring segment where the effective width and the effective permittivity are identical to the effective quantities for the microstrip lines [11]. Hence, no discontinuities by which nonexisting modes could be excited are introduced by the modified curved waveguide model. The model effective radius is given by

$$R_e = \frac{R}{2} + \frac{1}{2}\sqrt{R^2 + (w_e - w)w_e}. \tag{1}$$

Manuscript received September 18, 1989; revised May 29, 1990. This work was supported in part by the Raytheon/TI joint venture MIMIC Phase I Program.

The authors are with the Department of Electrical and Computer Engineering, Oregon State University, Corvallis, OR 97331.

IEEE Log Number 9037681.

0018-9480/90/1000-1449$01.00 ©1990 IEEE

The above effective radius ensures a positive value of the effective inner radius $r_{i,e}$, which approaches zero as the microstrip inner radius goes to zero (Fig. 2). As in the case with the waveguide modeling of the right-angle bend, the T junction, and other discontinuities [8], a correction corresponding to the difference in electrical length of the waveguide model and the actual structure must be made for accurate analysis of the curved bend.

The waveguide models assume that the substrate height h is small compared with the wavelength; hence, the fields are constant in the x direction. Thus, only a TEM mode and TE_{n0} modes with transversal components E_x and H_y exist inside the waveguides. The application of the mode-matching method given in [2] and [3] requires a complete set of transversal field solutions with orthogonal properties in all three regions. A complete set of solutions for the transversal field in regions I and II (i.e., in the straight waveguides) was derived in [3] and, for reference planes at $z=0$ and $z'=0$, is given by

$$E_x^{\mathrm{I}} = -\sum_{n=0}^{\infty}\sqrt{Z_n}\left(a_n^{\mathrm{I}}e^{-j\beta_n z}+b_n^{\mathrm{I}}e^{j\beta_n z}\right)\cdot\sqrt{\frac{\delta_n}{w_e h}}\cos\left[\frac{n\pi}{w_e}\left(y-\frac{w_e}{2}\right)\right]$$

$$H_y^{\mathrm{I}} = -\sum_{n=0}^{\infty}\sqrt{Y_n}\left(a_n^{\mathrm{I}}e^{-j\beta_n z}-b_n^{\mathrm{I}}e^{j\beta_n z}\right)\cdot\sqrt{\frac{\delta_n}{w_e h}}\cos\left[\frac{n\pi}{w_e}\left(y-\frac{w_e}{2}\right)\right] \tag{2a}$$

$$E_x^{\mathrm{II}} = -\sum_{n=0}^{\infty}\sqrt{Z_n}\left(a_n^{\mathrm{II}}e^{j\beta_n z'}+b_n^{\mathrm{II}}e^{-j\beta_n z'}\right)\cdot\sqrt{\frac{\delta_n}{w_e h}}\cos\left[\frac{n\pi}{w_e}\left(y-\frac{w_e}{2}\right)\right]$$

$$H_y^{\mathrm{II}} = \sum_{n=0}^{\infty}\sqrt{Y_n}\left(a_n^{\mathrm{II}}e^{j\beta_n z'}-b_n^{\mathrm{II}}e^{-j\beta_n z'}\right)\cdot\sqrt{\frac{\delta_n}{w_e h}}\cos\left[\frac{n\pi}{w_e}\left(y-\frac{w_e}{w}\right)\right] \tag{2b}$$

with

$$\delta_n = \begin{cases} 1 & \text{for } n=0 \text{ (TEM mode)} \\ 2 & \text{for } n>0 \text{ (TE}_{n0}\text{ modes)} \end{cases} \tag{2c}$$

and

$$\beta_n^2 = k_e^2 - \frac{n^2\pi^2}{w_e^2}, \qquad k_e^2 = \mu_0\epsilon_e\omega^2. \tag{2d}$$

Here β_n is the phase constant, $Z_n = 1/Y_n = \omega\mu_0/\beta_n$ is the characteristic wave impedance, and $a_n^{\mathrm{I}}, b_n^{\mathrm{I}}$ and $a_n^{\mathrm{II}}, b_n^{\mathrm{II}}$ are the normalized wave amplitudes.

In region III the wave equation and boundary conditions for $E_n = E_{x,n}$ in the curved orthogonal coordinate system as characterized by $u_1 = x$, $u_2 = y$, and $u_3 = s = R_e\varphi$ with corresponding metric coefficients $h_1 = h_2 = 1$ and $h_3 = 1 + y/R_e$ are given as [4], [12]

$$\left(1+\frac{y}{R_e}\right)^2\frac{\partial^2 E_n}{\partial y^2} + \frac{1}{R_e}\left(1+\frac{y}{R_e}\right)\frac{\partial E_n}{\partial y} + \frac{\partial^2 E_n}{\partial s^2} + k_e^2\left(1+\frac{y}{R_e}\right)^2 E_n = 0 \tag{3a}$$

and

$$\frac{\partial E_n}{\partial y} = 0 \qquad \text{at} \qquad y = \pm\frac{w_e}{2}. \tag{3b}$$

The solutions for E_n are expressed as

$$E_n = \left(1+\frac{y}{R_e}\right)\psi_n(y)e^{-j\tilde{\beta}_n s}. \tag{4a}$$

These form a complete set of eigenfunctions which are orthogonal with respect to the weighting function $(1+y/R_e)^{-1}$ [4], i.e.,

$$\int_{-w_e/2}^{w_e/2} E_m E_n\left(1+\frac{y}{R_e}\right)^{-1} dy = 0 \qquad \text{for } m \neq n. \tag{4b}$$

The orthogonality property for the functions $\psi_n(y)$ then immediately follows from (4a):

$$\int_{-w_e/2}^{w_e/2}\psi_m(y)\psi_n(y)\left(1+\frac{y}{R_e}\right)dy = 0 \qquad \text{for } m \neq n. \tag{5}$$

The total field strength E_x with unknown coefficients c_n is given by

$$E_x = \sum_{n=0}^{\infty} c_n E_n = \left(1+\frac{y}{R_e}\right)\sum_{n=0}^{\infty} c_n\psi_n(y)e^{-j\tilde{\beta}_n s}. \tag{6}$$

The magnetic field is readily found in terms of E_x from Maxwell's equations. For the transverse magnetic field component H_y we get

$$H_y = -\frac{1}{j\omega\mu_0}\left(1+\frac{y}{R_e}\right)^{-1}\frac{\partial E_x}{\partial s} = \frac{1}{\mu_0\omega}\sum_{n=0}^{\infty} c_n\tilde{\beta}_n\psi_n(y)e^{-j\tilde{\beta}_n s}. \tag{7}$$

A perturbation solution for the electromagnetic field can be found by expanding E_n and $\tilde{\beta}_n^2$ along s in a power series in the effective radius of curvature R_e of the curved waveguide as shown in [4] for a curved waveguide with electric walls:

$$E_n = e^{-j\tilde{\beta}_n s}\left(\phi_{0,n} + \frac{\phi_{1,n}}{R_e} + \frac{\phi_{2,n}}{R_e^2} + \cdots\right) = \left(1+\frac{y}{R_e}\right)\psi_n(y)e^{-j\tilde{\beta}_n s} \tag{8a}$$

$$\tilde{\beta}_n^2 = \beta_n^2\left(1 + \frac{B_{1,n}}{R_e} + \frac{B_{2,n}}{R_e^2} + \cdots\right). \tag{8b}$$

The quantities $\phi_{0,n}$ and β_n are the solutions for a straight waveguide ($R_e \to \infty$) and are given by

$$\phi_{0,n} = \cos\left[\frac{n\pi}{w_e}\left(y - \frac{w_e}{2}\right)\right] \tag{9a}$$

$$\beta_n^2 = k_e^2 - \frac{n^2\pi^2}{w_e^2}, \qquad k_e^2 = \mu_0\epsilon_e\omega^2. \tag{9b}$$

Substituting (8a) and (8b) into (3a) and comparing like powers of R_e leads to the solution for the expansion functions $\phi_{1,n}, \phi_{2,n}, \cdots$ and expansion constants $B_{1,n}, B_{2,n}, \cdots$, as shown by Lewin *et al.* [4]. The degree of accuracy and the complexity of the expressions obviously depend on the number of terms used in the expansions. For a second-order solution the expansion functions $\phi_{1,n}$ and $\phi_{2,n}$ as well as the phase constant $\tilde{\beta}_n$ are given as [4]

and

$$E_x^b = \left(1 + \frac{y}{R_e}\right)\sum_{n=0}^{\infty} c_n^b\psi_n \cos\left[\beta_n(s - R_e\alpha)\right]$$

$$H_y^b = \frac{1}{j\omega\mu_0}\sum_{n=0}^{\infty} c_n^b\tilde{\beta}_n\psi_n \sin\left[\tilde{\beta}_n(s - R_e\alpha)\right]. \tag{11b}$$

The coefficients c_n^a and c_n^b can be found by applying a normal mode-matching procedure in the same manner as in [2] and [3] to the continuity of the tangential magnetic field expressions at the boundaries between regions I and III and regions II and III as given by

$$H_y^{\mathrm{I}}(z=0) = H_y^b(s=0) \tag{12a}$$

and

$$H_y^{\mathrm{II}}(z'=0) = H_y^a(s = R_e\alpha). \tag{12b}$$

$$\phi_{1,n} = \begin{cases} k_e^2 y\left(\dfrac{w_e^2}{4} - \dfrac{y^2}{3}\right) & \text{for } n=0 \\[2ex] \dfrac{w_e^2}{2n^2\pi^2}\left\{\dfrac{d\phi_{0,n}}{dy}\left[\beta_n^2\left(y^2 - \dfrac{w_e^2}{4}\right) - \dfrac{k_e^2w_e^2}{n^2\pi^2}\right] - k_e^2 y\phi_{0,n}\right\} & \text{for } n>0 \end{cases} \tag{10a}$$

$$\phi_{2,n} = \begin{cases} \dfrac{k_e^2y^2}{6}\left[2y^2 - w_e^2 + \dfrac{k_e^2}{60}\left(6w_e^4 - 15y^2w_e^2 + 8y^4\right)\right] & \text{for } n=0 \\[2ex] p_n(y)\cdot\phi_{0,n} + q_n(y)\dfrac{d\phi_{0,n}}{dy} & \text{for } n>0 \end{cases} \tag{10b}$$

with

$$p_n(y) = \frac{w_e^2y^2}{8n^2\pi^2}\left[k_e^2\left(\frac{7k_e^2w_e^2}{n^2\pi^2} - 4\right) + \beta_n^4\left(\frac{w_e^2}{2} - y^2\right)\right]$$

and

$$q_n(y) = \frac{yw_e^4}{48n^4\pi^4}\left[12k_e^2\left(\frac{7k_e^2w_e^2}{n^2\pi^2} - 4\right) + \beta_n^2\left(w_e^2 - 4y^2\right)\left(9k_e^2 - 4\beta_n^2\right)\right]$$

$$\tilde{\beta}_n^2 = \begin{cases} k_e^2\left[1 - \dfrac{w_e^2}{12R_e^2}\left(1 - \dfrac{2}{5}k_e^2w_e^2\right)\right] & \text{for } n=0 \\[2ex] k_e^2\left(1 - \dfrac{n^2\pi^2}{k_e^2w_e^2}\right) + \dfrac{\pi^2}{6R_e^2}\left[n^2 + \dfrac{12 - n^2\pi^2}{2n^2\pi^4}k_e^2w_e^2 - \dfrac{21 + n^2\pi^2}{2n^4\pi^6}k_e^4w_e^4\right] & \text{for } n>0. \end{cases} \tag{10c}$$

A form of the field solution in region III which is suitable for the mode-matching method can be constructed by superimposing the field solutions obtained by alternately placing a magnetic wall at $s=0$ (E_x^a, H_y^a) and $s = R_e\alpha$ (E_x^b, H_y^b) [2], [3]:

$$E_x^a = \left(1 + \frac{y}{R_e}\right)\sum_{n=0}^{\infty} c_n^a\psi_n\cos\left(\tilde{\beta}_n s\right)$$

$$H_y^a = \frac{1}{j\omega\mu_0}\sum_{n=0}^{\infty} c_n^a\tilde{\beta}_n\psi_n\sin\left(\tilde{\beta}_n s\right) \tag{11a}$$

This leads to

$$c_n^a = \frac{j\omega\mu_0}{\tilde{\beta}_n I_n \sin\left(\tilde{\beta}_n R_e\alpha\right)}\sum_{p=0}^{\infty}\sqrt{Y_p}\left(a_p^{\mathrm{II}} - b_p^{\mathrm{II}}\right)\sqrt{\frac{\delta_p}{w_e h}}K(p,n) \tag{13a}$$

$$c_n^b = \frac{j\omega\mu_0}{\tilde{\beta}_n I_n \sin\left(\tilde{\beta}_n R_e\alpha\right)}\sum_{p=0}^{\infty}\sqrt{Y_p}\left(a_p^{\mathrm{I}} - b_p^{\mathrm{I}}\right)\sqrt{\frac{\delta_p}{w_e h}}K(p,n) \tag{13b}$$

with

$$I_n = \int_{-w_e/2}^{w_e/2}\psi_n^2(y)\left(1 + \frac{y}{R_e}\right)dy \tag{13c}$$

and

$$K(p,n)=\int_{-w_e/2}^{w_e/2}\phi_{0,p}(y)\psi_n(y)\left(1+\frac{y}{R_e}\right)dy. \quad (13d)$$

The continuity of the tangential electric field at the boundaries between regions I and III and regions II and III is expressed as

$$E_x^{\mathrm{I}}(z=0)=E_x^a(s=0)+E_x^b(s=0) \quad (14a)$$

and

$$E_x^{\mathrm{II}}(z'=0)=E_x^a(s=R_e\alpha)+E_x^b(s=R_e\alpha). \quad (14b)$$

Applying the mode-matching procedure to (14a) and (14b) leads to

$$(a_n^{\mathrm{I}}+b_n^{\mathrm{I}})\sqrt{\frac{Z_n w_e}{\delta_n h}} = -\sum_{m=0}^{\infty}\left[c_m^a+c_m^b\cos(\tilde{\beta}_m R_e\alpha)\right]K(n,m) \quad (15a)$$

and

$$(a_n^{\mathrm{II}}+b_n^{\mathrm{II}})\sqrt{\frac{Z_n w_e}{\delta_n h}} = -\sum_{m=0}^{\infty}\left[c_m^a\cos(\tilde{\beta}_m R_e\alpha)+c_m^b\right]K(n,m). \quad (15b)$$

The coefficients c_n^a and c_n^b can then be eliminated by inserting (13a) and (13b) into (15a) and (15b). Thus, an infinite set of linear equations for the wave amplitudes $a_n^{\mathrm{I}}, b_n^{\mathrm{I}}$ and $a_n^{\mathrm{II}}, b_n^{\mathrm{II}}$ is obtained. In order to obtain numerical results, this infinite set of equations is truncated to $2M+2$ equations, where M is the highest-order mode to be considered.

The scattering parameters S_{ij} for an incident TEM mode can be found by setting $a_n^{(j)}=1$ for $n=0$ and $j=1$ or 2, with all other $a_n^{(j)}$'s set equal to 0. Then the scattering parameters $S_{ij}=S_{ji}$ are given by

$$S_{ij}=b_0^{(i)} \quad (16)$$

where $b_0^{(i)}$ can be determined with standard routines for solving a set of linear equations.

III. Results

The transmission characteristics of typical curved microstrip bends have been computed, and good convergence with increasing number of higher order modes has been found. A typical convergence plot is shown in Fig. 3. As seen in this example, a minimum of three higher order modes must usually be considered in order to obtain a negligible truncation error. In the results for the curved microstrip bends presented in this paper, seven higher order modes were taken into account to ensure a negligible truncation error. Figs. 4–6 show the magnitudes of the scattering parameters of three different curved microstrip bends with $\alpha=90°$ and $R/w=2$ (Fig. 1), all normalized with respect to the microstrip impedance. Included in each figure are the scattering parameters of the corresponding right-angle and chamfered right-angle bends, characterized by the empirical CAD expressions given in [7] or by the magnetic wall waveguide model given in [8] and [9]. Fig. 4 shows the results for a nominal 50 Ω MMIC line on a 100 μm semi-insulating GaAs substrate. The results for the nominal 50 Ω and 35 Ω microstrip

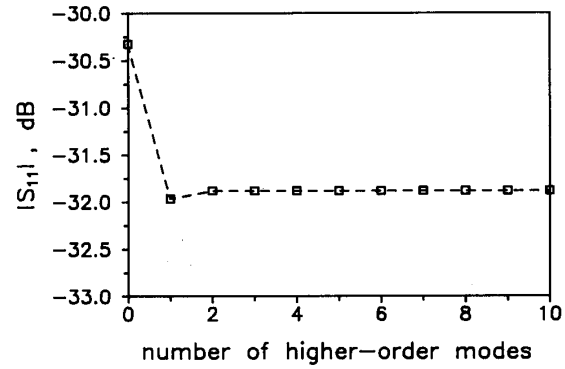

Fig. 3. Magnitude of the reflection coefficient as a function of the number of higher order modes at $f=30$ GHz for a curved microstrip bend with $\alpha=90°$, $R/w=2$, $w=73$ μm, $h=100$ μm, and $\epsilon_r=12.9$.

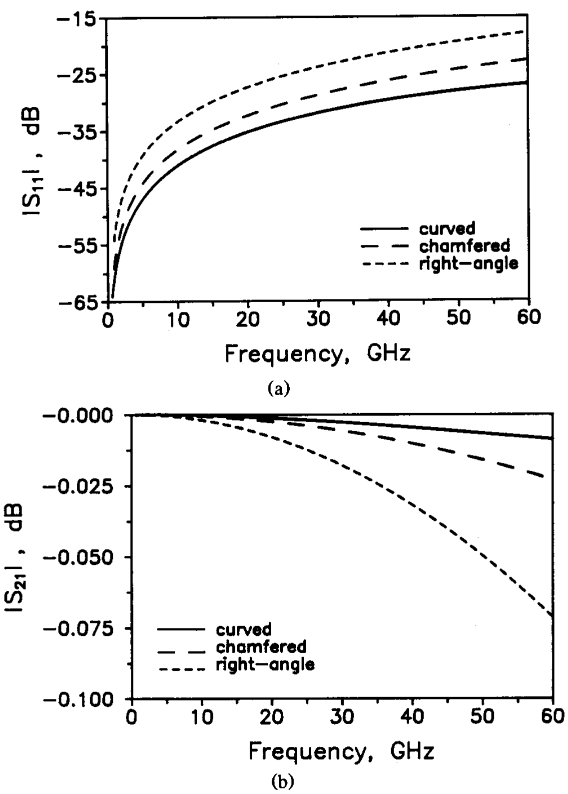

Fig. 4. Magnitude of (a) the reflection coefficient and (b) the transmission coefficient as a function of frequency for a curved microstrip bend with $\alpha=90°$ and $R/w=2$, a chamfered right-angle bend [7], and a right-angle bend [7]. $w=73$ μm, $h=100$ μm, and $\epsilon_r=12.9$ ($Z=50$ Ω).

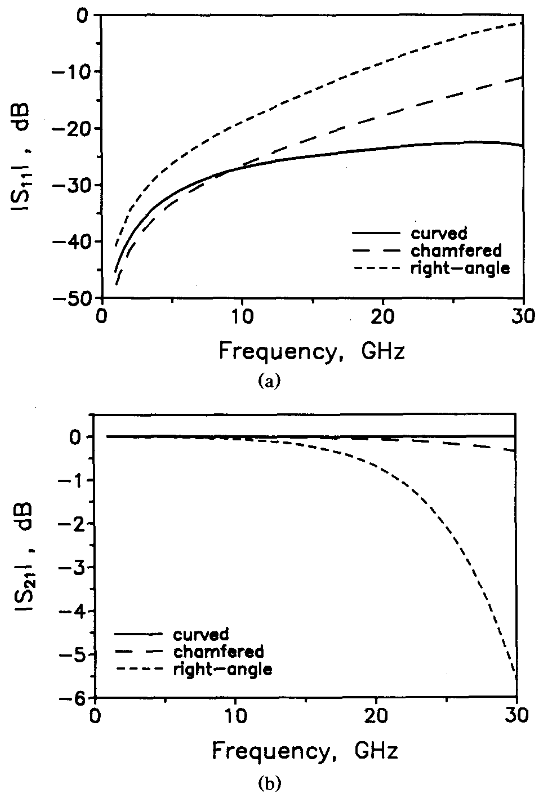

Fig. 5. Magnitude of (a) the reflection coefficient and (b) the transmission coefficient as a function of frequency for a curved microstrip bend with $\alpha = 90°$ and $R/w = 2$, a chamfered right-angle bend [9], and a right-angle bend [8]. $w = 0.6$ mm, $h = 0.635$ mm, and $\epsilon_r = 9.8$ ($Z = 50\ \Omega$).

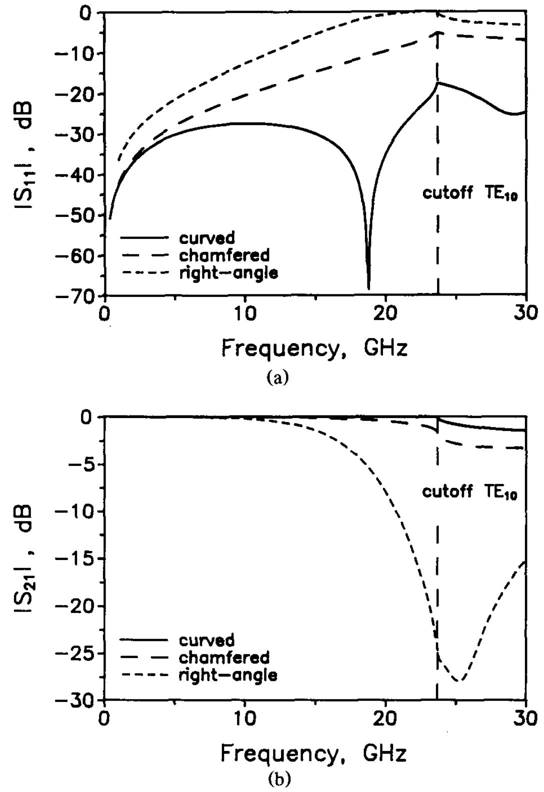

Fig. 6. Magnitude of (a) the reflection coefficient and (b) the transmission coefficient as a function of frequency for a curved microstrip bend with $\alpha = 90°$ and $R/w = 2$, a chamfered right-angle bend [9], and a right-angle bend [8]. $w = 1.2$ mm, $h = 0.635$ mm, and $\epsilon_r = 9.8$ ($Z = 35\ \Omega$).

lines on a 0.635 mm alumina substrate are shown in Figs. 5 and 6, respectively. In all three cases an improvement in the transmission properties with respect to the right-angle and chamfered right-angle bends is apparent, particularly for high frequencies.

It should be noted that the accuracy of these second-order perturbation solutions depends on the curvature R_e (or R_e/w_e) of the curved waveguide model; higher order terms may need to be included, especially when the inner radius of the microstrip goes to zero (i.e., $R/w \to 0.5$). However, the first-order perturbation solutions for the microstrip ring resonator as given in [12] are very close to the exact solutions computed in [11] for a wide range of parameters; therefore a corresponding superior accuracy of the second-order perturbation solutions is expected here including the results shown in Figs. 4–6. In addition, for moderate microstrip curvature, e.g. $R = w$ and $2w$, the results based on the waveguide model presented in this paper are in good agreement with experimental data for microstrip curved bends on thin GaAs substrates [13]. The reflection coefficient as a function of the radius of curvature and the angle for a nominal 50 Ω MMIC line on a 100 μm semi-insulating GaAs substrate is shown in Figs. 7 and 8.

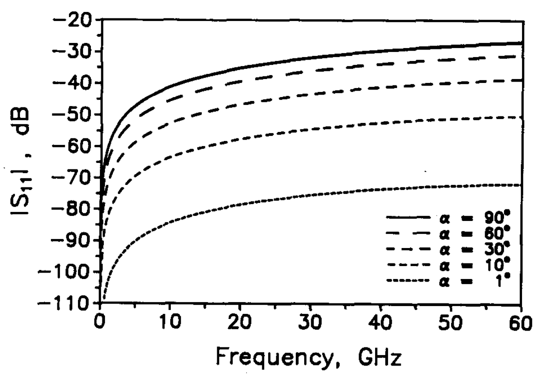

Fig. 7. Magnitude of the reflection coefficient as a function of frequency for a curved microstrip bend with $R/w = 2$, $w = 73$ μm, $h = 100$ μm, $\epsilon_r = 12.9$ ($Z = 50\ \Omega$), and various angles α.

IV. Conclusion

A method for calculating the frequency-dependent scattering parameters of curved microstrip bends has been described and computational results have been presented. The results have been compared with those obtained for the right-angle and the chamfered right-angle bends and

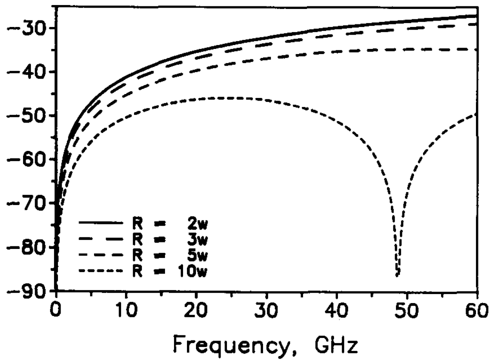

Fig. 8. Magnitude of the reflection coefficient as a function of frequency for a curved microstrip bend with $\alpha = 90°$, $w = 73$ μm, $h = 100$ μm, $\epsilon_r = 12.9$ ($Z = 50$ Ω), and various radii R.

show an improvement in the transmission properties. The results for the scattering parameters of the curved microstrip bend converge very fast with increasing number of higher order modes considered and have been shown to be consistent for large curvatures and bends with small angle.

REFERENCES

[1] G. Kompa and R. Mehran, "Planar waveguide model for microstrip discontinuities and T-junctions," *Electron. Lett.*, vol. 11, pp. 459–460, Sept. 1975.

[2] E. Kühn, "A mode-matching method for solving field problems in waveguide and resonator circuits," *Arch. Elek. Übertragung.*, vol. 27, pp. 511–513, Dec. 1973.

[3] W. Menzel and I. Wolff, "A method for calculating the frequency dependent properties of microstrip discontinuities," *IEEE Trans. Microwave Theory Tech.*, vol. MTT-25, pp. 107–112, Feb. 1977.

[4] L. Lewin *et al.*, *Electromagnetic Waves and Curved Structures.* New York: IEEE Press, 1977.

[5] H. Zucker and G. I. Cohn, "Propagation of TE modes in nonuniform waveguides," *IRE Trans. Microwave Theory Tech.*, vol. MTT-10, pp. 202–208, May 1962.

[6] E. Bahar and G. Govindarajan, "Rectangular and annular modal analysis of multimode waveguide bends," *IEEE Trans. Microwave Theory Tech.*, vol. MTT-21, pp. 819–824, Dec. 1972.

[7] M. Kirschning, R. H. Jansen, and N. H. L. Koster, "Measurement and computer-aided modeling of microstrip discontinuities by an improved resonator method," in *IEEE MTT-S Int. Microwave Symp. Dig.*, 1983, pp. 495–497.

[8] I. Wolff, "The waveguide model for the analysis of microstrip discontinuities," in *Numerical Techniques for Microwave and Millimeter-Wave Passive Structures*, Ed. New York: Wiley, 1989, ch. 7, pp. 447–495.

[9] W. Menzel, "Frequency-dependent transmission properties of truncated microstrip right-angle bends," *Electron. Lett.*, vol. 12, p. 641, Nov. 1976.

[10] M. Kirschning and R. H. Jansen, "Accurate wide-range design equations for the frequency-dependent characteristic of parallel coupled microstrip lines," *IEEE Trans. Microwave Theory Tech.*, vol. MTT-32, pp. 83–90, Jan. 1984.

[11] I. Wolff and V. K. Tripathi, "The microstrip open-ring resonator," *IEEE Trans. Microwave Theory Tech.*, vol. MTT-32, pp. 102–107, Jan. 1984.

[12] V. K. Tripathi and I. Wolff, "Perturbation analysis and design equations for open- and closed-ring microstrip resonators," *IEEE Trans. Microwave Theory Tech.*, vol. MTT-32, pp. 405–410, Apr. 1984.

[13] A. Weisshaar *et al.*, "Modeling of radial microstrip bends," in *IEEE MTT-S Int. Microwave Symp. Dig.*, May 1990, pp. 1051–1054.

Andreas Weisshaar received the M.S. degree in electrical and computer engineering from Oregon State University in 1986 and the Diplom-Ingenieur degree in electrical engineering in 1987 from the University of Stuttgart, in West Germany. He is currently a Research Assistant at Oregon State University and is completing work toward the Ph.D. degree in electrical and computer engineering. His current interests are in the computational techniques and modeling of radio wave propagation and general guided wave structures for MIMIC's, quantum waveguides, and integrated optics.

Vijai K. Tripathi (M'68–SM'87) received the B.Sc. degree from Agra University, Uttar Pradesh, India, in 1958, the M.Sc. Tech. degree in electronics and radio engineering from Allahabad University, Uttar Pradesh, India, in 1961, and the M.S.E.E. and Ph.D. degrees in electrical engineering from the University of Michigan, Ann Arbor, in 1964 and 1968, respectively.

From 1961 to 1963, he was a Senior Research Assistant at the Indian Institute of Technology, Bombay, India. In 1963, he joined the Electron Physics Laboratory of the University of Michigan, where he worked as a Research Assistant from 1963 to 1965 and as a Research Associate from 1966 to 1967 on microwave tubes and microwave solid-state devices. From 1968 to 1973, he was an Assistant Professor of Electrical Engineering at the University of Oklahoma, Norman. In 1974, he joined Oregon State University, Corvallis, where he is a Professor of Electrical and Computer Engineering. His visiting and sabbatical appointments have included the Division of Network Theory at Chalmers University of Technology in Gothenburg, Sweden, from November 1981 through May 1982; Duisburg University, Duisburg, West Germany, from June through September 1982; and the Electronics Technology Division of the Naval Research Laboratory in Washington, DC, in the summer of 1984. His current research activities are in the areas of microwave circuits and devices, electromagnetic fields, and solid-state devices.

Dr. Tripathi is a member of Eta Kappa Nu and Sigma Xi.

射 频 和 天 线 设 计 培 训 课 程 推 荐

易迪拓培训(www.edatop.com)由数名来自于研发第一线的资深工程师发起成立，致力并专注于微波、射频、天线设计研发人才的培养；我们于 2006 年整合合并微波 EDA 网(www.mweda.com)，现已发展成为国内最大的微波射频和天线设计人才培养基地，成功推出多套微波射频以及天线设计经典培训课程和 ADS、HFSS 等专业软件使用培训课程，广受客户好评；并先后与人民邮电出版社、电子工业出版社合作出版了多本专业图书，帮助数万名工程师提升了专业技术能力。客户遍布中兴通讯、研通高频、埃威航电、国人通信等多家国内知名公司，以及台湾工业技术研究院、永业科技、全一电子等多家台湾地区企业。

易迪拓培训课程列表：http://www.edatop.com/peixun/rfe/129.html

射频工程师养成培训课程套装

该套装精选了射频专业基础培训课程、射频仿真设计培训课程和射频电路测量培训课程三个类别共 30 门视频培训课程和 3 本图书教材；旨在引领学员全面学习一个射频工程师需要熟悉、理解和掌握的专业知识和研发设计能力。通过套装的学习，能够让学员完全达到和胜任一个合格的射频工程师的要求…

课程网址：http://www.edatop.com/peixun/rfe/110.html

ADS 学习培训课程套装

该套装是迄今国内最全面、最权威的 ADS 培训教程，共包含 10 门 ADS 学习培训课程。课程是由具有多年 ADS 使用经验的微波射频与通信系统设计领域资深专家讲解，并多结合设计实例，由浅入深、详细而又全面地讲解了 ADS 在微波射频电路设计、通信系统设计和电磁仿真设计方面的内容。能让您在最短的时间内学会使用 ADS，迅速提升个人技术能力，把 ADS 真正应用到实际研发工作中去，成为 ADS 设计专家...

课程网址： http://www.edatop.com/peixun/ads/13.html

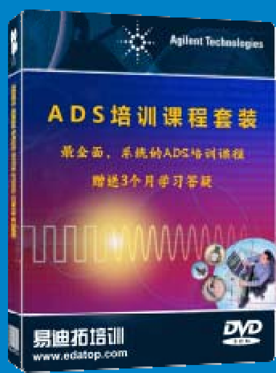

HFSS 学习培训课程套装

该套课程套装包含了本站全部 HFSS 培训课程，是迄今国内最全面、最专业的 HFSS 培训教程套装，可以帮助您从零开始，全面深入学习 HFSS 的各项功能和在多个方面的工程应用。购买套装，更可超值赠送 3 个月免费学习答疑，随时解答您学习过程中遇到的棘手问题，让您的 HFSS 学习更加轻松顺畅…

课程网址：http://www.edatop.com/peixun/hfss/11.html

CST 学习培训课程套装

该培训套装由易迪拓培训联合微波 EDA 网共同推出，是最全面、系统、专业的 CST 微波工作室培训课程套装，所有课程都由经验丰富的专家授课，视频教学，可以帮助您从零开始，全面系统地学习 CST 微波工作的各项功能及其在微波射频、天线设计等领域的设计应用。且购买该套装，还可超值赠送 3 个月免费学习答疑…

课程网址：http://www.edatop.com/peixun/cst/24.html

HFSS 天线设计培训课程套装

套装包含 6 门视频课程和 1 本图书，课程从基础讲起，内容由浅入深，理论介绍和实际操作讲解相结合，全面系统的讲解了 HFSS 天线设计的全过程。是国内最全面、最专业的 HFSS 天线设计课程，可以帮助您快速学习掌握如何使用 HFSS 设计天线，让天线设计不再难…

课程网址：http://www.edatop.com/peixun/hfss/122.html

13.56MHz NFC/RFID 线圈天线设计培训课程套装

套装包含 4 门视频培训课程，培训将 13.56MHz 线圈天线设计原理和仿真设计实践相结合，全面系统地讲解了 13.56MHz 线圈天线的工作原理、设计方法、设计考量以及使用 HFSS 和 CST 仿真分析线圈天线的具体操作，同时还介绍了 13.56MHz 线圈天线匹配电路的设计和调试。通过该套课程的学习，可以帮助您快速学习掌握 13.56MHz 线圈天线及其匹配电路的原理、设计和调试…

详情浏览：http://www.edatop.com/peixun/antenna/116.html

我们的课程优势：

※ 成立于 2004 年，10 多年丰富的行业经验，

※ 一直致力并专注于微波射频和天线设计工程师的培养，更了解该行业对人才的要求

※ 经验丰富的一线资深工程师讲授，结合实际工程案例，直观、实用、易学

联系我们：

※ 易迪拓培训官网：http://www.edatop.com

※ 微波 EDA 网：http://www.mweda.com

※ 官方淘宝店：http://shop36920890.taobao.com